

Effect of Preparation Parameters on Physical, Thermal and Optical Properties of n-type Porous Silicon

Kasra Behzad*, Wan Mahmood Mat Yunus, Zainal Abidin Talib, Azmi Zakaria and Afarin Bahrami

Department of Physics, Science Faculty, Universiti Putra Malaysia, 43400 UPM Serdang, Selangor, Malaysia.

*E-mail: kasra.behzad@gmail.com

Received: 4 April 2012 / Accepted: 2 August 2012 / Published: 1 September 2012

Porous silicon (PSi) layers were formed on n-type silicon (Si) wafers using electrochemical etching method. The effects of etching time and current density were investigated. Three sets of samples were prepared at different current densities: 10, 20, and 30 mA/cm² and six etching times: 10, 20, 30, 40, 50, and 60 min. The thickness and porosity of the layers were measured using the gravimetric method. The surface morphology was studied by Field Emission Scanning Electron Microscope (FESEM). The optical and thermal properties of porous silicon on silicon substrates were investigated by employing photoluminescence (PL) and photoacoustic spectroscopy (PAS). Thermal results showed that the thermal diffusivity (TD) of samples decrease with increasing the porosity. The band gap of the samples were obtained from photoluminescence (PL) and photoacoustic absorption spectra. These results showed that the band gap of porous silicon samples increase with increasing porosity.

Keywords: Porous silicon, Electrochemical etching, Porosity, Photoacoustic spectroscopy, Thermal diffusivity, Photoluminescence.

1. INTRODUCTION

Porous silicon (PSi) was discovered in 1956 by Uhir [1] while performing electropolishing experiments on silicon wafers, using an electrolyte containing hydrofluoric acid (HF). Under the appropriate applied current and solution composition, the silicon remained uniformly undissolved, but rather fine holes were produced. PSi formation was obtained by electrochemical dissolution of silicon wafers in aqueous or ethanoic HF solutions. In the 1970s and 1980s, interest in PSi increased because its high surface area was found to be useful as a model of the crystalline silicon surface in spectroscopic studies [2], as a precursor to generate thick oxide layers on silicon, and as a dielectric layer in capacitance based chemical sensors. In the 1990s Leigh Canham published his results on red

luminescence [3] from PSi, and explained it in terms of quantum confinement of carriers in nanocrystals of silicon present on the pore walls. The discovery of efficient visible light emission from PSi was followed by an explosion of work focused on creating silicon-based optoelectronic switches, displays, and lasers. During the last twenty years, the optical properties of PSi have become a very intense area for research [4]. Porous silicon is a promising material due to the excellent optical, mechanical, and thermal properties, obvious compatibility with silicon-based microelectronics [5] and the low cost. The large surface area within a small volume, controllable pore sizes, convenient surface chemistry, and the ability to modulate refractive index as a function of depth [6] makes PSi a suitable dielectric material for multilayers [7]. All these features also lead, on one hand, to interesting optical properties via mixing silicon with air in an effective medium approximation; PSi has been given considerable attention for solar cell and sensor applications [8, 9]. Its luminescence properties, large surface area, and compatibility with silicon-based devices are reasons that for PSi implementation in sensors and the solar cells. Related to these applications, the ability of adjustment and control of certain parameters have more importance. The band gap and thermal diffusivity are such parameters in sensors, solar cells [10], electronic [11] and optoelectronic [12] devices, thermal flow sensors [13], isolators [14] and fuel cells [15]. In this study, we investigated the band gap, absorbance and the thermal diffusivity of n-type porous silicon (PSi) samples prepared by electrochemical etching method, under varying current density and etching time. The structural properties were studied by FESEM and the optical properties investigated by employing photoluminescence (PL) and photoacoustic spectroscopy (PAS). PAS was also carried out to measure the thermal diffusivity of PSi samples. Several earlier studies [16-18] considered the physical properties, photoluminescence (PL), absorption spectra, band gap and thermal diffusivity (TD) of PSi samples. Unlike those studies that considered only one preparation parameter such as etching time, current density or volume ratio of electrolyte separately, this paper investigated the effects of both etching time and current density as variable factors simultaneously on the physical, optical and thermal properties of PSi.

2. MATERIALS AND METHODS

2.1. Sample preparation

All the samples were formed on (100) n-type silicon single crystal wafers of 520 μm thickness and 1-10 ohm.cm resistivity. The silicon (Si) sample was placed in the bottom of cylindrical Teflon cell and fixed by an aluminium plate as a backing material. A platinum rod, as cathode, was placed perpendicular to the Si surface at a distance of 1 cm. The samples were obtained by varying the current density and etching time at a concentration of 48-50% HF, 99.90% ethanol (HF:C₂H₅OH) in the volume ratio of 1:1. A DC current source (ADCMT 6243) was used to supply a constant current. The samples were prepared under 10 mA/cm², 20 mA/cm², and 30 mA/cm² current densities and the etching time of 10, 20, 30, 40, 50, and 60 min.

2.2. Characterisations

FESEM (Nova NanoSEM 30 series) was used to investigate the surface morphology. Thickness and porosity of the samples were calculated by the gravimetric method [4, 19]. The samples are weighted before etching (m_1), after etching (m_2), and after dissolution of the PSi layer in a molar NaOH aqueous solution (m_3). The porosity and thickness were calculated by the following equations respectively:

$$P(\%) = \frac{m_1 - m_2}{m_1 - m_3} \times 100 \quad (1)$$

$$d = \frac{m_1 - m_3}{\rho S} \quad (2)$$

where ρ and S are the Si density and the etched surface area, respectively. The thickness of the PSi layers also was measured by a stylus profilometer (Ambios Technology, XP-200). PSi-based structures have been shown to luminesce in the NIR, visible and near UV. Accordingly, the PL results are in the visible field, a so-called S-band [20]. The S-band's large spectral width results from inhomogeneous broadening and its spectral position depends on porosity [4]. Photoluminescence spectroscopy was performed by Fluorescence Spectrometer (Perkin Elmer, LS-55) at room temperature with an excitation wavelength of 410 nm. PAS was used to determine the optical absorption and the thermal diffusivity - the rate of heat energy diffusion into a material. Two different PAS setups were used to characterize the samples: chopping frequency dependence setup, in order to measure the thermal diffusivity (TD) and fixed chopping frequency setup to obtain the absorbance spectra and calculate the band gap. All PAS setups consisted of three parts: light source, detector, and data analysing system. For the chopping frequency dependant photoacoustic (PA) signal, a Melles Griot HeNe laser of 632.8 nm at power of 75 mW was used as a light source that was modulated through a mechanical chopper.

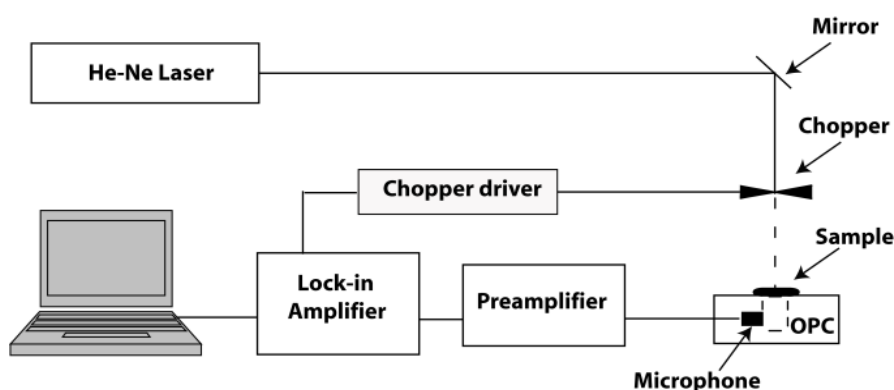


Figure 1. Schematic diagram of the chopping frequency dependence PAS setup.

As shown in Figure 1, an open photoacoustic cell (OPC) was used as a detector. The preamplifier (Stanford Research Systems, SR560) was utilized to amplify the output signal from OPC

and transmit it to a lock-in amplifier (Stanford Research Systems, SR530). A Lab VIEW program controlled the setup via a GPIB bus [21].

Theoretical analysis of the PAS has been reviewed in several previous studies [22-24]. Based on the PA theory, the amplitude (S) of PA spectra in the thermally thick region varies as:

$$S = \frac{A}{f} \exp(-b\sqrt{f}) \quad , \quad b = (\pi l_s^2 / \alpha_s)^{1/2} \quad (3)$$

where, f is chopping frequency, l_s is sample thickness and α_s is thermal diffusivity (TD) of the sample, thus

$$\alpha_s = \frac{k}{\rho C_p} \quad (4)$$

where, k is thermal conductivity, ρ is density and C_p is the specific heat of the sample.

Figure 2, shows the schematic diagram of the fixed chopping frequency PAS setup. The HeNe laser was replaced by 300 W Xenon arc lamp and a monochromator. The PA spectra were measured and analyzed for an excitation energy range from 300 to 800 nm (1.5 - 4.13 eV) and a modulation frequency of 73 Hz. According to the Tauc relation, $(\alpha h\nu)^n = \beta(h\nu - E_g)$ and extrapolating the data for $(\alpha h\nu)^n = 0$, the band gap value was determined for each sample [25].

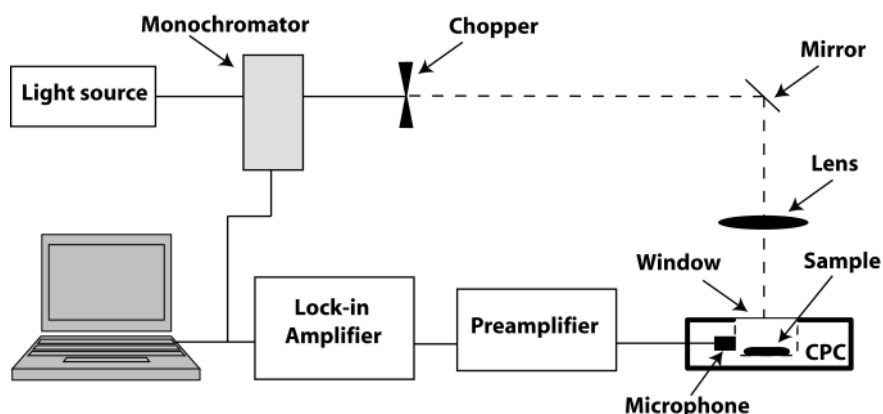


Figure 2. Schematic diagram of fix chopping frequency PAS setup.

3. RESULTS

3.1. Physical Properties

Figure 3 shows a typical FESEM image of the etched surface prepared under current density of 30 mA/cm² and etching time of 40 min with pore size ranging from 400 nm to 1600 nm. The bright regions in the figure are the Si structures and the dark regions the pores. By increasing the porosity of the P*S*i layers, Si structures decrease while the size of the pores increases.

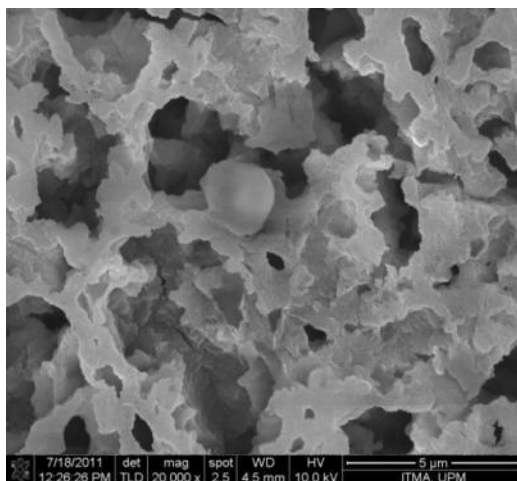


Figure 3. FESEM image of n-type porous silicon surface ($J=30 \text{ mA/cm}^2$ and $t=40 \text{ min}$).

The percent porosity and thickness of the layers were calculated using the Eq. 1 and Eq. 2. As shown in the Figure 4a, the average thickness of PSi layers raises linearly by increasing the etching time for each set of samples. The thicknesses of the samples measured by stylus profilometer are in complete agreement with the gravimetric results. Figure 4b shows that the porosity initially increases rapidly, and then roughly levels off after reaching 45 min. The published studies confirmed porosity and thickness increase by increasing the etching time or current density in n-type PSi layers [26, 27].

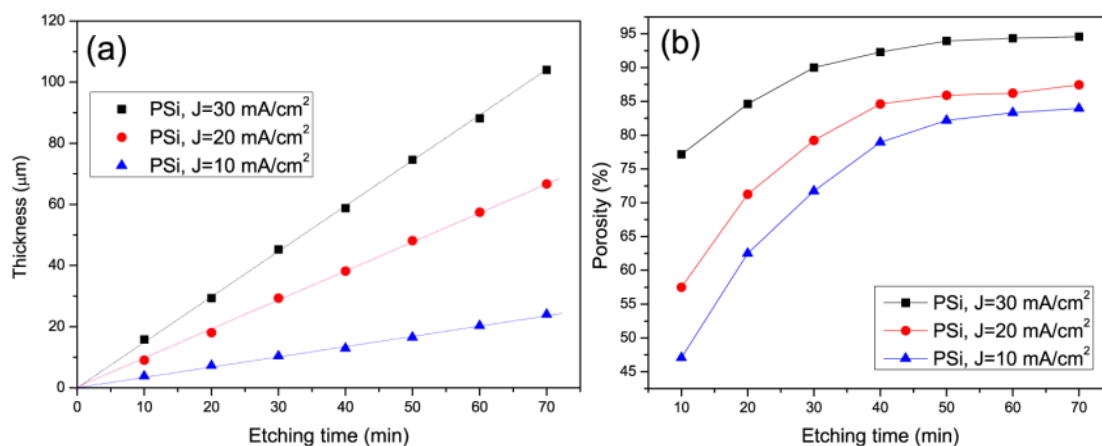


Figure 4. a) Thickness as a function of etching time, b) Porosity as a function of etching time.

3.2. Photoluminescence (PL)

The PL emission peaks of samples were measured at room temperature. Figure 5a shows typical PL curves of the samples obtained at current density of 10 mA/cm^2 , and different etching times. The PL peaks are related to the S-band emission, and the peaks show a blue shift with increasing the etching time/porosity in each set.

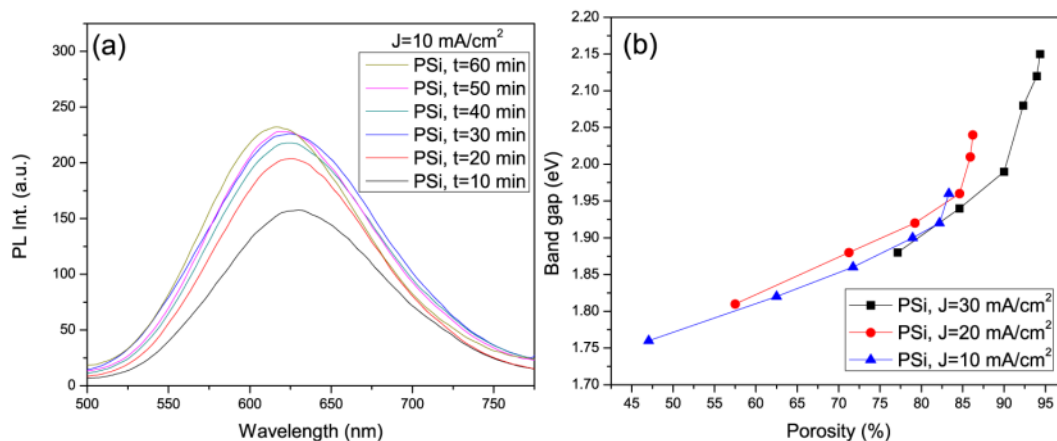


Figure 5. a) PL peaks for PSi samples prepared under a fix current density ($J=10 \text{ mA/cm}^2$) and different etching time, b) Band gap vs. porosity extracted from PL spectroscopy for PSi samples.

As we have studied earlier, the porosity increases with increasing etching time. The silicon structure size on the surface clearly decreases by increasing the porosity. Size dependency of the PL energy, which explains the efficient luminescence, causes the peaks to shift towards the lower wavelength or higher energy, as already reported [4, 28]. According to the particle in a box theory as the size of box (L) changes, the allowed energy changes proportionally as $1/L^2$, hence the allowed energies increase with decreasing size of box. The band gap energy versus porosity is shown in Figure 5b. In this study, the band gap increased from 1.76 to 2.15 eV by increasing the current density (10 - 30 mA/cm^2) and etching time (10 - 60 min). For all samples, the band gap value increased with increasing the porosity due to change in the Si structure size. The extracted values of band gap are in the same range of the reported results (1.5-2.5 eV) for PSi samples [9, 16, 23].

3.3. Photoacoustic Spectroscopy (PAS)-Chopping Frequency Dependent

Figure 6a shows the PA signal of a PSi/Si sample in the thermally thick region and the fitting line with Eq. 3. The variations of the TD are compared and shown in Figure 6b. The results show that the TD of PSi samples are significantly lower than that of the silicon sample ($\alpha_{Si} \cong 0.9 \text{ cm}^2/\text{s}$). In each set with a common current density, the TD decreases by increasing the porosity, because of the reduction in the mean free path, due to the phonon confinement in the crystallite. This reduction is caused by a limitation of the phonon mean free path due to scattering at boundaries of the large inner surface of PSi [29]. TD values of the samples decrease from 0.33 to 0.08 cm^2/s by increasing the porosity from 47% to 94%. Based on preparation conditions, a wide range of the TD values have been reported for PSi samples, which decrease by increasing the porosity [30, 31]. These results confirm the probability of thermal insulation by the PSi/Si structure in contrast to c-Si, which has a higher TD. This result can be useful in designing the silicon based devices.

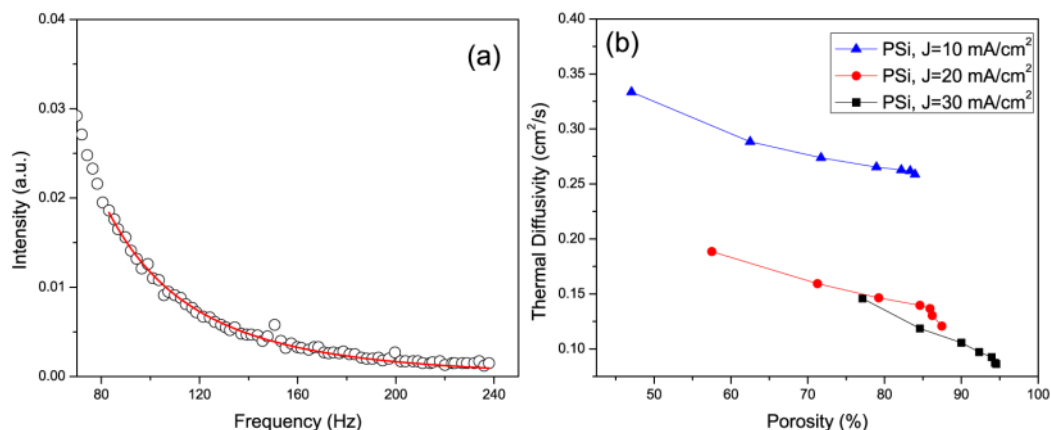


Figure 6. a) PA signal for a PSi/Si sample ($J=30 \text{ mA/cm}^2$, $t=40 \text{ min}$) under the chopping frequency in thermally thick region. The solid curve represents the best fit of the experimental data to eq. 3, b) Variation of TD vs. porosity of the PSi samples obtained at different current densities and etching times.

3.4. Photoacoustic Spectroscopy (PAS)-Fix Chopping Frequency

The PA intensity is proportional to the optical absorption of the sample [32]. The PAS spectra of the samples were obtained by recording the PA signal as a function of wavelength with incident beam ranging from 300 to 800. The PA spectra were normalized using the spectrum obtained from carbon black powder. Figure 7 shows the normalized PA spectra for one set of samples prepared at 30 mA/cm^2 . The graphs show that the optical absorption reaches a maximum value around 350 nm and then decreases with increasing the wavelength.

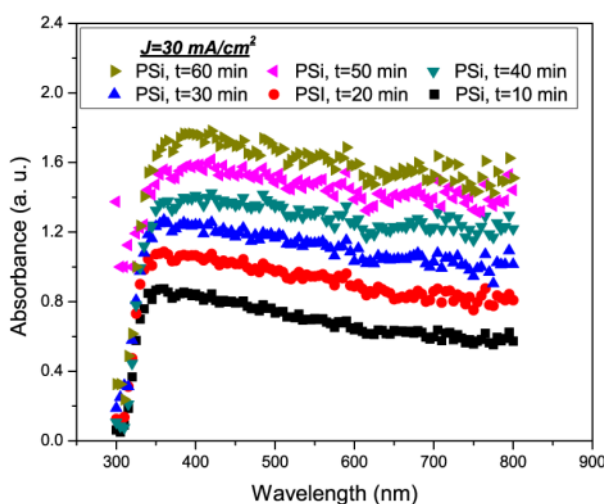


Figure 7. The PA intensity spectra of PSi samples prepared at 30 mA/cm^2 with different etching time.

These results indicate a stronger quantum confinement of the carriers in the PSi layers, which is due to the smaller dimensions of PSi structures as compared to Si crystallites. The optical absorption was plotted versus the incident photon energy, and the value of the band gap energy was determined by extrapolating the linear part of the graph. Figure 8a shows $(\alpha h\nu)^2$ versus energy for one set of

samples. Each graph was extrapolated for $(\alpha h\nu)^2 = 0$ to find the related band gap. The calculated band gaps of the samples are plotted in Figure 8b. This figure demonstrates that the band gap energy can be tuned with etching time or porosity for different applications. These band gap values are agreed with the values obtain from PL measurement with $\pm 2\%$.

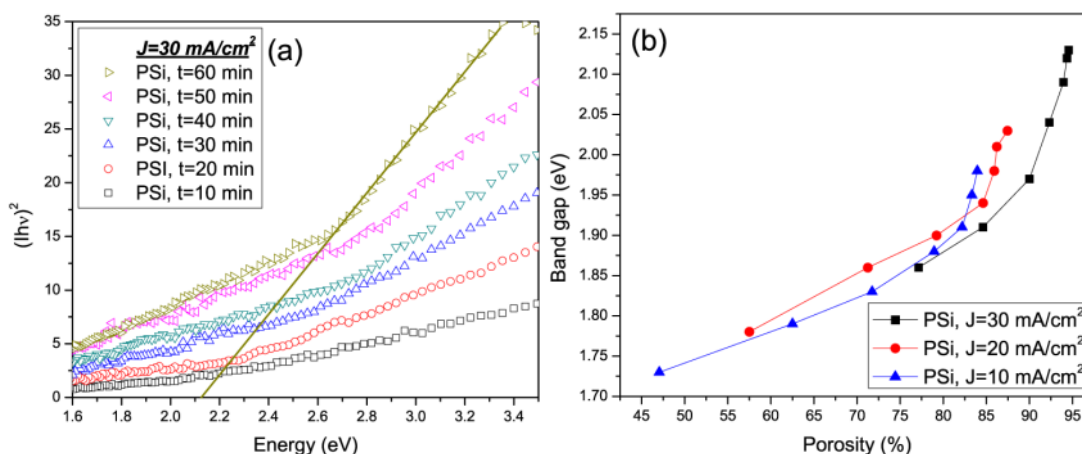


Figure 8. a) $(Ih\nu)^2$ versus energy for one set of PSi samples, b) Band gap vs. Porosity for all samples.

4. CONCLUSIONS

In summary, PSi samples were prepared by electrochemical etching method under three current densities and six different etching times. We have studied the dependence of the thickness and porosity of samples on the current density and etching time. The results show that the porosity increases rapidly and then remains approximately constant, whereas the overall thickness of the PSi layer grows linearly in time. The thickest layer shows more porosity due to the extra dissolution of PSi layer. By increasing the porosity, the size of the Si structures in PSi layer reduce, which affects the properties of PSi layers. The PL shows a gradually blue shift in peaks with increasing etching time that is due to changes of the Si structure size in the PSi layers. Using the PL and PAS, it was found that the band gap value increased with increasing the porosity. The band gap results from these two methods are in a good agreement. The results show that the band gap becomes wider with increasing porosity. The PAS was also carried out to measure the TD. The TD was significantly smaller than that of the Si, and decreased with increased porosity, which is attributed to a decrease in the mean free path caused by the phonon confinement in crystallite. It was found that the optical and thermal properties depend strongly on the PSi structure. It is clear that by adjusting the etching time and current density, as prepared parameters, the thermal diffusivity and band gap energy can be controlled. These results indicate that the PSi is a good candidate for photonic devices.

ACKNOWLEDGEMENTS

The authors gratefully acknowledge the Department of Physics, UPM and Ministry of Higher Education for the financial support through Fundamental research grant (01-11-08-664FR/5523664 and 01-04-10-861FR/5523901).

References

1. A. Ulhir, AT&T TECH J, 35 (1956) 333.
2. A.C. Dillon, M.B. Robinson, M.Y. Han and S.M. George, *J Electrochem Soc*, 139 (1992) 537-543.
3. L.T. Canham, *Adv Mater*, 7 (1995) 1033-1037.
4. O. Bisi, S. Ossicini and L. Pavesi, *Surf Sci Rep*, 38 (2000) 1-126.
5. K.D. Hirschman, L. Tsybeskov, S.P. Duttagupta and P.M. Fauchet, *Nature*, 384 (1996) 338-341.
6. C.C. Striemer and P.M. Fauchet, *Appl Phys Lett*, 81 (2002) 2980-2982.
7. C. Mazzoleni and L. Pavesi, *Appl Phys Lett*, 67 (1995) 2983-2985.
8. S. Ozdemir and J.L. Gole, *Curr Opin Solid STM*, 11 (2007) 92-100.
9. M. Rajabi and R. Dariani, *J Porous Mat*, 16 (2009) 513-519.
10. N. Marrero, R. Guerrero-Lemus, B. Gonzalez-Diaz and D. Borchert, *Thin Solid Films*, 517 (2009) 2648-2650.
11. Y. Qu, L. Liao, Y. Li, H. Zhang, Y. Huang and X. Duan, *Nano Lett*, 9 (2009) 4539-4543.
12. R. Dubey and D. Gautam, *Opt Quant Electron*, 41 (2009) 189-201.
13. G. Kaltsas, A.A. Nassiopoulou and A.G. Nassiopoulou, *Sensors Journal*, IEEE, 2 (2002) 463-475.
14. D.N. Pagonis, A.G. Nassiopoulou and G. Kaltsas, *J Electrochem Soc*, 151 (2004) H174-H179.
15. T. Pichonat and B. Gauthier-Manuel, *J Power Sources*, 154 (2006) 198-201.
16. C.K. Sheng, W. Mahmood Mat Yunus, W.M.Z.W. Yunus, Z. Abidin Talib and A. Kassim, *Physica B*, 403 (2008) 2634-2638.
17. S. Alekseev, D. Andrusenko, R. Burbelo, M. Isaiev and A. Kuzmich, *J. Phys.: Conf. Ser.*, 278 (2011) 012003.
18. M. Malinski, L. Chrobak and L. Bychto, *Solid State Commun*, 150 (2010) 424-427.
19. A.S. Khaldun, Z. Hassan and K. Omar, *Int. J. Electrochem. Sci.*, 7 (2012) 376-386.
20. Z. Gaburro, N. Daldosoh, L. Pavesi, B. Franco, L.L. Gerald and W. Peter, *Porous Silicon*, in *Encyclopedia of Condensed Matter Physics*. 2005, Elsevier: Oxford. p. 391-401.
21. K. Behzad, W. Mahmood Mat Yunus, Z. Abidin Talib, A. Zakaria, A. Bahrami and E. Shahriari, *Advances in Optical Technologies*, 2012 (2012) 1-9.
22. K. Behzad, W.M. Mat Yunus, Z.A. Talib, A. Zakaria and A. Bahrami, *Materials*, 5 (2012) 157-168.
23. R. Srinivasan, M. Jayachandran and K. Ramachandran, *Cryst Res Technol*, 42 (2007) 266-274.
24. E. Ramachandran, P. Raji, K. Ramachandran and S. Natarajan, *Cryst Res Technol*, 41 (2006) 64-67.
25. J. Tauc and A. Menth, *J Non-Cryst Solids*, 8-10 (1972) 569-585.
26. S.D. Milani, R. Dariani, A. Mortezaali, V. Daadmehr and K. Robbie, *J. Optoelectron. Adv. M.*, 8 (2006) 1216-1220.
27. B. Cho, S. Jin, B.-Y. Lee, M. Hwang, H.-C. Kim and H. Sohn, *Microelectron. Eng.*, 89 (2011) 92-96.
28. T.P. Nguyen, P.L. Rendu, V.H. Tran, V. Parkhutik and R.F. Esteve, *J Porous Mat*, 7 (2000) 393-396.
29. J. Zou and A. Balandin, *J Appl Phys*, 89 (2001) 2932-2938.
30. Q. Shen and T. Toyoda, *J Therm Anal Calorim*, 69 (2002) 1067-1073.
31. U. Bernini, P. Maddalena, E. Massera and A. Ramaglia, *Optics Communications*, 168 (1999) 305-

314.

32. E. Ramachandran, P. Raji, K. Ramachandran and S. Natarajan, *Cryst Res Technol*, 41 (2006) 481-486.

© 2012 by ESG (www.electrochemsci.org)